



CHORUS

This is the accepted manuscript made available via CHORUS. The article has been published as:

Femtosecond Compression Dynamics and Timing Jitter Suppression in a THz-driven Electron Bunch Compressor

E. C. Snively, M. A. K. Othman, M. Kozina, B. K. Ofori-Okai, S. P. Weathersby, S. Park, X. Shen, X. J. Wang, M. C. Hoffmann, R. K. Li, and E. A. Nanni

Phys. Rev. Lett. **124**, 054801 — Published 4 February 2020

DOI: [10.1103/PhysRevLett.124.054801](https://doi.org/10.1103/PhysRevLett.124.054801)

Femtosecond compression dynamics and timing jitter suppression in a terahertz-driven electron bunch compressor

E. C. Snively,^{1,*} M. A. K. Othman,^{1,†} M. Kozina,¹ B. K. Ofori-Okai,¹ S. P. Weathersby,¹ S. Park,^{1,2} X. Shen,¹ X. J. Wang,¹ M. C. Hoffmann,^{1,‡} R. K. Li,^{1,§} and E. A. Nanni^{1,¶}

¹*SLAC National Accelerator Laboratory, 2575 Sand Hill Road, Menlo Park, California, 94025, USA*

²*Stanford Institute for Materials and Energy Sciences,*

SLAC National Accelerator Laboratory, Menlo Park, CA 94025, USA

We present the first demonstration of THz-driven bunch compression and timing stabilization of a relativistic electron beam. Quasi-single-cycle strong field THz radiation is used in a shorted parallel-plate structure to compress a few-fC beam with 2.5 MeV kinetic energy by a factor of 2.7, producing a 39 fs rms bunch length and a reduction in timing jitter by more than a factor of 2 to 31 fs rms. This THz-driven technique offers a significant improvement to beam performance for applications like ultrafast electron diffraction, providing a critical step towards unprecedented timing resolution in ultrafast sciences and other accelerator applications using femtosecond-scale electron beams.

PACS numbers:

Advances in electron-beam based ultrafast science continue to reach unprecedented sensitivity, with techniques like pump-probe ultrafast electron diffraction (UED) achieving sub-angstrom spatial resolution and temporal resolutions down to 100 fs using electron bunch lengths of only tens of femtoseconds [1–3]. The intense demand for ever shorter high-brightness electron beams has ignited a campaign to achieve fs-scale bunch lengths and timing stability through beam-wave interactions at THz frequencies [4–9], following the advent of THz-based accelerator technology [10–13]. THz-driven compression techniques in the relativistic regime, where space-charge effects are suppressed, could potentially enable production of high-brightness ultra-short bunches with sufficient charge to capture single shot images in UED, allowing characterization of irreversible processes at the time scale of atomic motion [14, 15]. Bunch compression techniques using conventional radio frequency (RF) structures have succeeded in producing ultralow emittance few-fs beams [16] and represent a significant step towards achieving the high-brightness beams needed for single-shot UED. However, RF-based acceleration and manipulation suffer from phase jitter, on the order of tens to hundreds of femtoseconds depending on the drive source stability [17–19], causing time-of-arrival (TOA) jitter between electron beam and reference pump laser.

THz-driven beam manipulation has been recognized as a promising candidate in the pursuit of few-fs beams with sub-fs timing resolution, because the inherent timing synchronization of all-optical control enables both bunch compression and reduction of beam timing jitter. Already, THz-driven beam manipulation has demonstrated dramatic compression in the sub-relativistic regime (<100 keV electrons), reaching bunch lengths of tens of femtoseconds while reducing the timing jitter to

a few femtoseconds [4, 6, 9]. Beyond the synchronization benefit that comes with a laser-driven interaction, structures operating in the THz regime offer a host of advantages. For applications like bunch compression or transverse deflection, the higher frequency provides a more efficient time-dependent momentum kick compared to conventional RF manipulation. Using sub-wavelength structures for localized field enhancement [20], THz-driven streaking diagnostics have already demonstrated femtosecond, down to sub-femtosecond metrology of relativistic beams [21, 22]. Additionally, the sub-mm length scale of the THz regime enables the use of small-footprint structures supporting strong synchronism for efficient beam manipulation while occupying only mm-scale space on the beamline.

We present the results of a THz-driven compression experiment performed at the SLAC MeV-UED facility at SLAC National Accelerator Laboratory using a shorted parallel-plate waveguide (PPWG) design [23]. Both the manipulation and characterization of the relativistic electron beam were accomplished through interaction with quasi-single-cycle THz pulses generated via optical rectification of 800 nm laser pulses [24]. Using the shorted PPWG to couple the relativistic electron beam and an orthogonally propagating < 3 μ J THz pulse, we produced a beam energy chirp resulting in compression by a factor of 2.7, with a minimum bunch length of 39 ± 7 fs rms. An equally important consequence of this interaction is the simultaneous improvement to the beam's shot-to-shot TOA (rms) stability by a factor of > 2.5, reducing the timing jitter to 31 fs rms for the case of maximum compression. This THz-driven compression experiment builds on the success of the THz-based streaking diagnostic developed at SLAC MeV-UED, which previously demonstrated sub-fs rms timing accuracy of few MeV

beams [22]. The THz-driven bunch compression and timing stabilization setup is integrated with the THz-driven beam diagnostic, as shown in Fig. 1. The enhanced capabilities of these combined technologies are uniquely positioned to be directly applied to UED experiments.

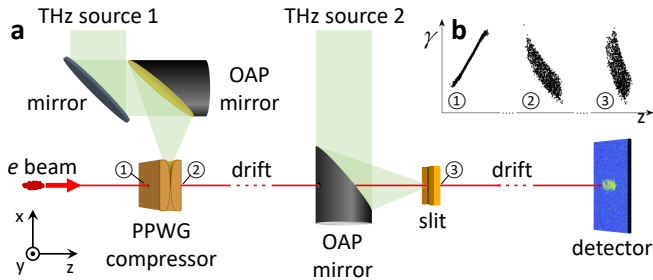


FIG. 1: (a) Schematic of the in-vacuum components for the THz-driven compression and streaking setup. Within the PPWG compressor, coupling between the electron beam and THz pulse reverses the beam’s energy chirp, resulting in velocity bunching during the subsequent drift. (b) Snapshots of the simulated longitudinal phase space (electron energy γ vs. z -position) are shown for the beam 1) entering the compressor, 2) exiting the compressor, and 3) at the streaking slit. In the slit, the second THz pulse imparts a transverse momentum kick to the beam which streaks the longitudinal profile onto the y -axis on a downstream imaging detector. THz source 1 is polarized along the z -axis; THz source 2 is polarized along the y -axis.

The Ti:Sapphire laser system at SLAC MeV-UED provided a 13 ± 1 mJ, near-IR (800 nm) pulse at 180 Hz which was split to drive the UV source, producing up to few-hundred nJ pulses for electron beam generation in the S-band photocathode gun, and two separate THz sources, in which the pulse-front-tilt method was used for optical rectification in LiNbO₃ crystals [25, 26]. A 70-30 beam splitter directed the primary IR pulse to THz source 1, for compression, and the secondary pulse to THz source 2 for streaking, with translation stages controlling each path length for timing adjustment. The optical components of THz source 1 were mounted to a vertical breadboard, producing a horizontally polarized quasi-single-cycle pulse with $\sim 0.05\%$ conversion efficiency. A pair of off-axis parabolic (OAP) mirrors collimated and then focused the pulse into the compressor horn. Downstream, THz source 2 produced a vertically polarized pulse with $\sim 0.1\%$ conversion efficiency, which was transported to the streaking setup using OAPs. A 2.5 mm hole allowed beam transmission through the final OAP, which brought the THz pulse into collinear propagation as it was focused into the metallic PPWG “slit” of the streaking structure [22], see Fig. 1a.

The 2.856 GHz photocathode gun supplied a relativistic electron beam with 2.5 MeV kinetic energy and sub-10 fC total charge. After initial collimation with a focusing solenoid, the beam was aligned through a pinhole and then focused with a second solenoid to a $\sim 40 \mu\text{m}$ rms

spot size in the compressor. The bunch length and timing jitter of the uncompressed beam were 105 ± 19 fs rms and 76 fs rms, respectively, measured by the THz-driven streaking diagnostic 1 m downstream of the compressor.

The THz-driven compression technique presented here utilized a PPWG structure that benefits from two key design enhancements. Where the THz pulse entered the structure, an exponentially-tapered adiabatic horn [23] was matched to the free-space THz beam profile, improving the coupling efficiency and allowing dispersion-free focusing of the THz pulse into the PPWG at the center of the structure. The adiabatic horn, shown in Fig. 2, focused the z -component of the THz pulse as it propagated along the x -axis, overcoming the free space diffraction limit and providing nearly two-fold field enhancement between the parallel plates aligned in the x - y plane. A copper short, located at the edge of the beam tunnel ($125 \mu\text{m}$ from beam axis) within the PPWG, produced a superposition of forward and reflected THz field in the vicinity of the passing electron beam, increasing the parallel electric field driving the energy chirp, while reducing the magnetic field which imparted an undesirable transverse momentum kick.

The integrated Lorentz force experienced by particles at different positions along the bunch length was determined by the temporal overlap with the THz field as the electron beam traversed the PPWG gap. Ideally, the beam was injected at a phase with maximum electric field

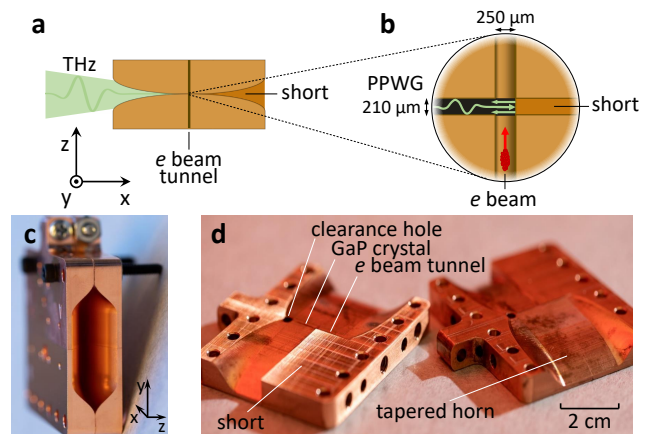


FIG. 2: (a) Diagram of the compressor cross-section, with incoming THz pulse polarized along the z -axis. (b) Close-up view of the interaction region, showing the $250 \mu\text{m}$ diameter beam tunnel and the $210 \mu\text{m}$ PPWG gap. A short reflects the incoming THz pulse. (c) Photograph of the assembled structure showing the adiabatic horn opening. (d) Photograph of the disassembled structure before the final etch. The structure is translated along the y -axis to switch between compressor “on” with beam passing through the beam tunnel and compressor “off” with beam passing through the 2.54 mm diameter clearance hole. A GaP crystal was used for in-situ electro-optic (EO) sampling of the THz field.

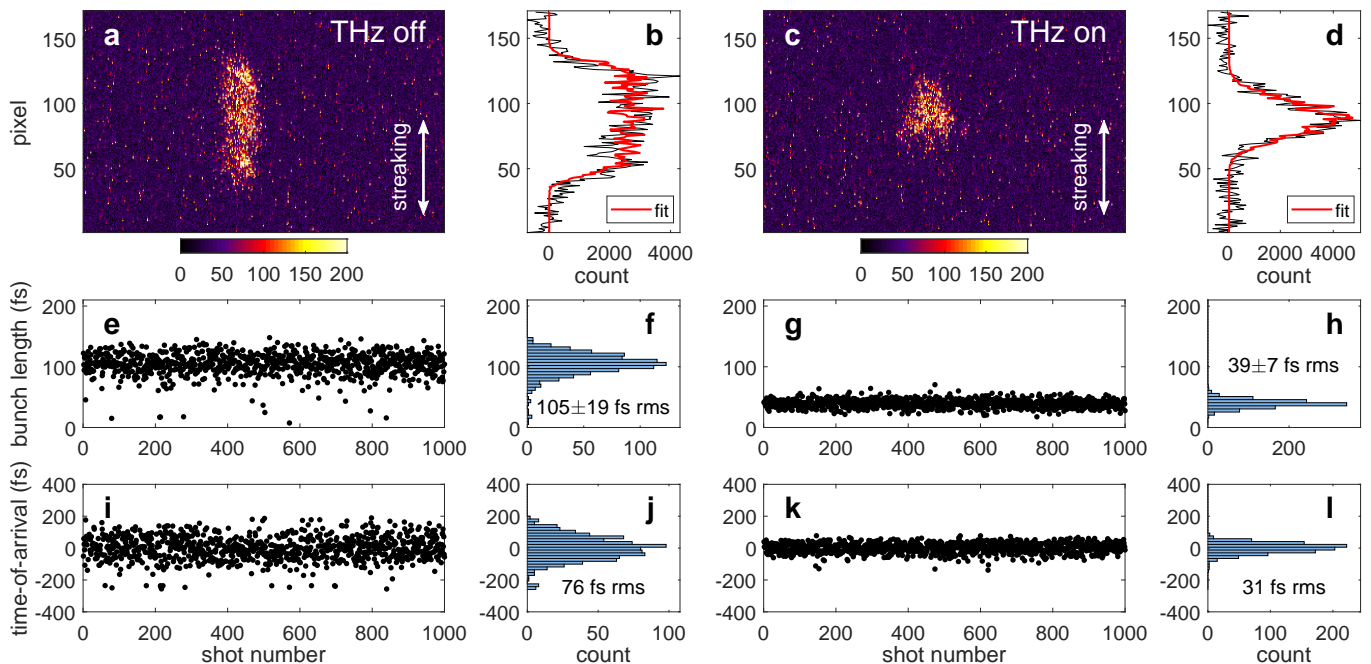


FIG. 3: Comparison of the uncompressed beam to the maximally compressed beam. Single shot beam images in (a) and (c) show examples with THz-driven compression “off” and “on”, respectively, with the corresponding fit to their projected distribution shown in (b) and (d). (e)-(f) show the rms bunch length of the uncompressed beam over 1000 shots, with a mean of 105 fs and standard deviation of 19 fs. (g)-(h) show the rms bunch length of the compressed beam over 1000 shots, with a mean of 39 fs and standard deviation of 7 fs. (i)-(j) show the time-of-arrival of the uncompressed beam over 1000 shots, with a timing jitter of 76 fs rms. (k)-(l) show the time-of-arrival of the compressed beam over 1000 shots, giving a reduced timing jitter of 31 fs rms.

gradient, typically near a zero-crossing in the waveform. Here, the beam acquires a near-linear longitudinal energy chirp with the correct sign for bunch compression, i.e. the energy of particles at the tail of the beam increase relative to particles at the head of the beam, as shown in Fig. 1b. This effect also causes the energy of a “late” bunch to increase relative to an “early” bunch. As a result, the compressor interaction reduced the shot-to-shot beam timing jitter after a subsequent drift. This effect relies on the inherent timing synchronization between the THz pulse and electron beam generated using the same initial laser pulse. For beams arriving far from the zero-crossing, the non-linearity of the energy chirp limits the achievable bunch compression.

The Lorentz force within the PPWG interaction region also produced a time-dependent transverse deflection of the beam. To reduce this deflection and defocusing caused by the magnetic field, the short was added to the PPWG design, resulting in constructive interference of the electric field while the magnetic field was partially canceled [23]. At the local maxima in deflection, the shot-to-shot beam pointing jitter increased to 30 μrad rms from the 10 μrad rms jitter without THz interaction. The interaction phase for maximum compression, near a local maximum in deflection, produced a shot-to-shot pointing jitter of up to 50 μrad rms. Steering mag-

nets placed after the compression chamber were used to compensate for deflection, ensuring consistent alignment through the streaking diagnostic. The small increase in pointing jitter and beam size due to time-dependent deflection could not be corrected with the quadrupole doublet. However, the rms distribution of integrated diffraction peaks did not increase enough to adversely affect the beam’s utility for applications like UED, as demonstrated with single-crystal gold used to characterize the electron beam energy.

For measurements of the electron bunch length and TOA, the longitudinal profile of the beam was projected onto the y-axis through the time-dependent transverse momentum kick imparted by the second THz pulse [22]. The direction and magnitude of the deflection was determined by the THz pulse’s temporal profile. A calibration of femtoseconds per pixel was obtained by scanning the THz arrival time and mapping the beam centroid position on the phosphor screen placed 2 m downstream. To extract the beam characteristics from a single shot image of the charge profile after streaking, we compare the measured distribution to a Gaussian longitudinal beam profile, as predicted by GPT simulations [27], mapped into a “projected distribution” using the known streaking calibration curve. The length and timestamp of the Gaussian distribution are allowed to vary to find the best

fit of the simulated distribution to the actual projected beam image. This method deals effectively with the irregular charge distributions produced when the initial longitudinal beam profile fills the region mapped out by the THz-driven transverse deflection, causing the charge to “pile-up” at the ends of the projected distribution.

In Figure 3a-d, we show examples of single shot beam images alongside their corresponding projected distribution, with the background subtracted, and the fit produced through the test beam method. An uncompressed bunch is shown at left; a maximally compressed bunch is shown at right. In Fig. 3e-l, the bunch length and TOA for 1000 shots of the uncompressed beam indicate a bunch length of 105 ± 19 fs rms and timing jitter of 76 fs rms. For 1000 shots of the compressed beam, the bunch length and timing jitter are reduced to 39 ± 7 fs rms and 31 fs rms, respectively. The factor of 2.5 reduction in timing jitter is slightly smaller than the measured compression factor of 2.7. However, similar measurements of 1000 shots taken at neighboring interaction phases near the minimum bunch length show timing jitters as low as 24 fs rms, see Fig. 4a, indicating a factor of 3.2 jitter reduction.

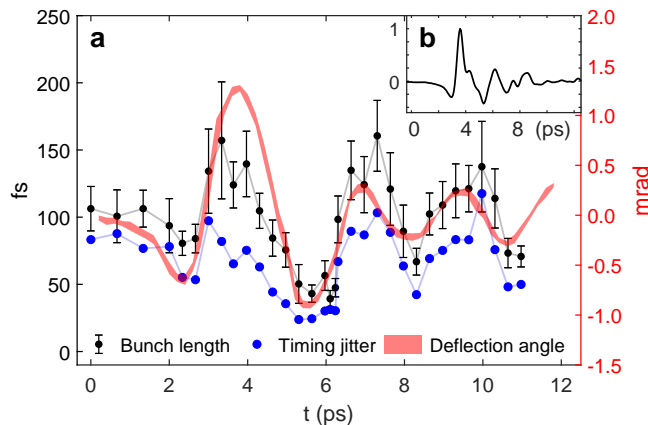


FIG. 4: (a) Scan of the bunch length and timing jitter of the electron beam, along with the deflection angle in the x-z plane (scale shown on right axis), as a function of the THz pulse arrival time within the compressor structure. The line width of the deflection data reflects the standard deviation of deflection angle. (b) EO sampling within the PPWG structure, characterizing the THz field in the un-shortened region. The ringing apparent after ~ 6 ps is an artifact from the EO crystal, not the true waveform.

The bunch length, timing jitter and transverse deflection of the beam varied according to the quasi-single-cycle profile of the driving THz field, as shown by the scan of THz arrival time in Fig. 4a, with each exhibiting a parallel change in sign and magnitude. Because the deflection of the beam necessitated realignment between each streaking measurement, the full set of bunch length and timing jitter measurements was acquired over several hours. During this time, a slow drift in the relative TOA

resulted in a cumulative scaling uncertainty on the order of 1 ps per hour. The deflection data was collected in a separate scan, independent of the streaking setup.

EO measurements of the THz pulse in the un-shortened section of PPWG, see Fig. 4b, were used to simulate the THz field in the shorted PPWG section with Ansoft HFSS software [23]. Using these field maps and the measured initial beam parameters, simulations performed in GPT show that the peak field sampled by the beam within the compressor must be around 100 MV/m in order to reproduce the compressed bunch length of 39 fs rms as measured at the streaking slit. This value is consistent with our expected field enhancement, given the THz pulse energy and structure design [23]. The simulation results indicate that maximum compression occurred approximately 70 cm downstream of the streaking slit at a minimum bunch length of ~ 32 fs rms. The compression achieved in our experiment was primarily limited by the available THz energy, with measurements further limited by the location of our streaking diagnostic. Eventually, this shorted PPWG compression technique would also be limited by the increase to the slice energy spread of the beam.

In simulation and measurement, the compressor-induced deflection is predominantly along the x-axis. The largest peaks in measured deflection along the y-axis coincided with peaks in the x-deflection, but with smaller magnitude, reaching only $250 \mu\text{rad}$ where the x-deflection peaked to 1.27 mrad. The magnitude of the measured y-deflection is consistent with simulations, but the GPT model predicts x-deflection that is a factor of two larger than observed in measurements. Differences in the position of the beam within the tunnel cross-section are a likely source of discrepancy between our measurements and simulation, causing the beam to sample a different region of the shorted field profile compared to the on-axis trajectory assumed in simulation. This inhomogeneity caused by the short in the PPWG structure is key to the reduction in the transverse deflection, and required optimization of the distance between the short and beam axis for the phase of the forward and reflected magnetic field to add destructively along the beam path [23]. Even within the optimal interaction region, GPT simulations indicate that variations in the field profile sampled by different portions of the beam are a major factor in the slice energy spread growth, reaching up to 0.6 keV rms, even as the overall energy spread of 1 keV rms can be kept low or actually decrease, as dictated by the chirp required for compression.

A dual feed structure utilizing counterpropagating THz pulses could also mitigate the transverse momentum kick while driving an energy chirp, as has been demonstrated [6] for a sub-relativistic beam. This method offers flexibility and fidelity of the THz field superposition, but introduces the additional challenge of requiring either a second THz source, or THz splitting op-

tics with additional beam transport. A single-feed horn with split waveguide design, in which the beam tunnel passes through two PPWG interaction regions, could provide added flexibility for optimization of the energy chirp while canceling the induced deflection and potentially improve the uniformity of the field, reducing the slice energy spread growth predicted for the current design.

In summary, we have shown a compression interaction, driven by a laser-generated THz pulse in a parallel plate waveguide, that reduces the bunch length while acting to correct the timing jitter of the relativistic beam, stabilizing its TOA with respect to a reference laser pulse. The simultaneous compression to a 39 fs rms bunch length and 31 fs rms timing jitter provides a significant benefit to performance for electron-beam based ultrafast science, given that the overall temporal resolution of a measurement is dependent on the bunch length and timing jitter added in quadrature. The transverse deflection of the beam induced by this compression interaction is easily corrected using steering magnets and introduces a minimal increase to the beam pointing jitter. The magnitude of compression achieved through this technique could be directly improved by increasing the THz field at the interaction point, with state-of-the-art THz sources already providing > 1 GV/m fields at source [29]. This demonstration of THz-driven compression and timing stabilization is a critical step towards achieving the ultra-short electron beams that could enable UED measurements at the attosecond scale. More broadly, electron beams conditioned through this technique would be advantageous for many accelerator applications, such as pump-probe ultrafast electron scattering and external injection in laser-driven accelerators, that demand few-fs timing stability and bunch lengths [30–32].

The authors acknowledge M. Cardoso, A. Sy, and A. Haase for structure fabrication. This research has been supported by the U.S. Department of Energy (DOE) under Contract No. DE-AC02-76SF00515. The SLAC MeV-UED program is supported in part by DOE Basic Energy Sciences (BES) Scientific User Facilities Division and SLAC UED/UEM program development: DE-AC02-05CH11231. M. K. and M. C. H. are supported by the DOE Office of Science, BES, award no. 2015-SLAC100238-Funding.

E. C. S., M. A. K. O., and M. K. contributed equally to this work.

* Electronic address: esnively@slac.stanford.edu

† Electronic address: mothman@slac.stanford.edu

‡ Electronic address: hoffmann@slac.stanford.edu

§ Electronic address: lirk@tsinghua.edu.cn

¶ Electronic address: nanni@slac.stanford.edu

[1] S. P. Weathersby, G. Brown, M. Centurion, T. F. Chase, R. Coffee, J. Corbett, J. P. Eichner, J. C. Frisch,

A. R. Fry, M. Gühr, and N. Hartmann. *Review of Scientific Instruments*, 86.7, (2015).

- [2] E. M. Mannebach, R. Li, K. A. Duerloo, C. Nyby, P. Zalden, T. Vecchione, F. Ernst, A. H. Reid, T. Chase, X. Shen, and S. Weathersby. *Nano letters*, 15(10), 6889-6895, (2015).
- [3] J. Yang, M. Guehr, T. Vecchione, M. S. Robinson, R. Li, N. Hartmann, X. Shen, R. Coffee, J. Corbett, A. Fry, and K. Gaffney. *Nature communications* 7, 11232, (2016).
- [4] C. Kealhofer, W. Schneider, D. Ehberger, A. Ryabov, F. Krausz, and P. Baum. *Science* **352**(6284), 429-433 (2016).
- [5] E. Curry, S. Fabbri, J. Maxson, P. Musumeci, and A. Gover, *Phys. Rev. Lett.* **120**(9), 094801 (2018).
- [6] D. Zhang, A. Fallahi, M. Hemmer, X. Wu, M. Fakhari, Y. Hua, H. Cankaya, A. L. Calendron, L. E. Zapata, N. H. Matlis, and F. X. Kärtner, *Nat. Photonics* **12**(6), 336 (2018).
- [7] L. Zhao, T. Jiang, C. Lu, R. Wang, Z. Wang, P. Zhu, Y. Shi, et al. *Phys. Rev. Accel. Beams* **21**(8), 082801 (2018).
- [8] D. Ehberger, A. Ryabov, and P. Baum. *Physical review letters* **121**(9), 094801 (2018).
- [9] D. Ehberger, K. J. Mohler, T. Vasileiadis, R. Ernstorfer, L. Waldecker, and P. Baum. *Physical Review Applied*, **11**(2), 024034 (2019).
- [10] L. J. Wong, A. Fallahi, and F. X. Kärtner. *Optics express* **21**(8), 9792-9806, (2013).
- [11] L. Wimmer, G. Herink, D. R. Solli, S. V. Yalunin, K. E. Echternkamp, and C. Ropers. *Nature Physics* **10**(6), 432, (2014).
- [12] E. A. Nanni, W. R. Huang, K. H. Hong, K. Ravi, A. Fallahi, G. Moriena, R. D. Miller, and F. X. Kärtner. *Nature communications* **6**, 8486, (2015).
- [13] W. R. Huang, A. Fallahi, X. Wu, H. Cankaya, A. L. Calendron, K. Ravi, D. Zhang, E. A. Nanni, K. H. Hong, and F. X. Kärtner. *Optica* **3**(11), 1209-1212, (2016).
- [14] G. Sciaini, and R. D. Miller. *Rep. Prog. Phys.* **74**(9), 096101 (2011).
- [15] E. Hall, S. Stemmer, H. Zheng, Y. Zhu, and G. Maracas. US Department of Energy, Washington, DC (United States), 2014.
- [16] J. Maxson, D. Cesar, G. Calmasini, A. Ody, P. Musumeci, and D. Alesini. *Phys. Rev. Lett.* **118**(15), 154802 (2017).
- [17] P. Craievich, S. Di Mitri, M. Milloch, G. Penco, and F. Rossi. *Physical Review Special Topics-Accelerators and Beams*, 16, no. 9 (2013): 090401.
- [18] R. Pompili, M. P. Anania, M. Bellaveglia, A. Biagioni, G. Castorina, E. Chiadroni, A. Cianchi, M. Croia, D. Di Giovenale, M. Ferrario, and F. Filippi. *New Journal of Physics*, 18, no. 8 (2016): 083033.
- [19] R. K. Li and C. X. Tang. *Nuclear Instruments and Methods in Physics Research Section A: Accelerators, Spectrometers, Detectors and Associated Equipment*, 605, no. 3 (2009): 243-248.
- [20] J. Fabiańska, G. Kassier and T. Feurer. *Scientific Reports* 4: 5645 (2014)
- [21] L. Zhao, Z. Wang, C. Lu, R. Wang, C. Hu, P. Wang, J. Qi, et al. *Phys. Rev. X* **8**(2), 021061 (2018).
- [22] R. K. Li, M. C. Hoffmann, E. A. Nanni, S. H. Glenzer, M. E. Kozina, A. M. Lindenberg, et al. *Phys. Rev. Accel. Beams* **22**(1), 012803 (2019).
- [23] M. A. K. Othman, M. C. Hoffmann, M. K. Kozina, X. J. Wang, R. K. Li, and E. A. Nanni. *Opt. Express* **27**,

- 23791 (2019).
- [24] B. K. Ofori-Okai, M. C. Hoffmann, A. H. Reid, S. Edstrom, R. K. Jobe, R. K. Li, E. M. Mannebach, et al. *J. Instrum.* **13**(06), P06014 (2018).
- [25] J. Hebling, G. Almasi, I. Z. Kozma, and J. Kuhl. *Opt. Express* **10**(21), 1161-1166 (2002).
- [26] J. A. Fülöp, L. Pálfalvi, M. C. Hoffmann, and J. Hebling. *Opt. Express* **19**(16), 15090-15097 (2011).
- [27] M. J. De Loos, and S. B. Van Der Geer. General Particle Tracer: A new 3D code for accelerator and beamline design. *In 5th European Particle Accelerator Conference*, (1996).
- [28] J. A. Fülöp, Z. Ollmann, C. Lombosi, C. Skrobol, S. Klingebiel, L. Pálfalvi, F. Krausz, S. Karsch, and J. Hebling. *Opt. Express* **22**(17), 20155-20163 (2014).
- [29] C. Vicario, B. Monozslai, and C. P. Hauri. *Physical Review Letters*, 112, no. 21 (2014): 213901.
- [30] V. Malka, J. Faure, Y. A. Gauduel, E. Lefebvre, A. Rousse, and K. T. Phuoc. *Nature physics*, 4(6), 447 (2008).
- [31] E. Esarey, C. B. Schroeder, and W. P. Leemans. *Reviews of modern physics*, 81, no. 3 (2009): 1229.
- [32] R. J. England, R. J. Noble, K. Bane, D. H. Dowell, C. K. Ng, J. E. Spencer, S. Tantawi, et al. *Reviews of Modern Physics* 86, no. 4 (2014): 1337.